ACS APPLIED MATERIALS & INTERFACES

www.acsami.org Research Article

Low Reducing Potentials Enabled by CaF_2-Supported Graphene Electrodes in High Impedance Solutions

Rifat Shahriar, Bofan Zhao, Indu Aravind, Zhi Cai, Yu Yun Wang, Boxin Zhang, and Stephen B. Cronin*

Cite This: https://doi.org/10.1021/acsami.4c09551 Read Online

ABSTRACT: We report electrochemical measurements using in situ Raman spectroscopy at graphene/D_2O interfaces under extremely low applied potentials. Here, the hydrophobic and catalytically inert nature of graphene and the insulating nature of the deionized (DI) water enables potentials as low as $V_{applied} = -7$ V vs Ag/AgCl to be applied without exceeding 200 $\mu A/cm^2$ of current density. At higher currents, bubble formation (i.e., hydrogen evolution reaction) prohibits reliable spectra from being obtained from the electrode surface. Using CaF_2 as the supporting substrate enables significantly lower reducing potentials to be reached compared to glass substrates, likely due to trapped charge and impurities in the glass substrate. G band Raman spectra taken under various applied electrochemical potentials exhibit a linear relationship between the G band shift ($\Delta\omega_G$) and the applied potential, with blueshifts as high as $\Delta\omega_G = 18$ cm^{-1}. These large Raman shifts indicate a large change in the Fermi level of $\Delta E_F = -0.43$ eV for graphene electrodes in contact with water, favoring reduction half-reactions. Based on the solution resistance measurement, there is a $V_{IR} = 3.1$ V voltage drop across the solution for D_2O (when the applied potential was $V_{applied} = -7$ V vs Ag/AgCl) and the effective reducing potential on the working electrode is $V_{effective} = -3.9$ V vs Ag/AgCl. We have also tested these graphene electrodes in ionic liquids [DEME][TFSI], which are limited to applied potentials above $V_{applied} = -2.7$ V vs Ag/AgCl and a corresponding shift in the Fermi level $\Delta E_F = -0.32$ eV, indicating that pure water can provide a more robust electrolyte for reaching low reducing potentials than ionic liquids.

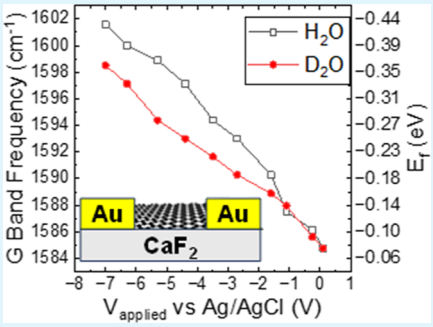

KEYWORDS: *graphene, low reducing potentials, high operating voltage window, ionic liquids, Raman spectroscopy*

■ INTRODUCTION

The behavior of water at charged interfaces plays an important role in a variety of chemical and biological processes ranging from electrocatalysis to biomembranes,[1−4] and assumes a crucial role in areas ranging from life sciences and environmental chemistry to heterogeneous catalysis, electrochemistry, and energy conversion applications. The solvation properties of interfacial water dictate chemical equilibria and reaction rates. Through the use of surfactants, the orientation of water at charged interfaces has been studied extensively using vibrational sum frequency generation spectroscopy (SFG).[4−9] Montenegro et al. observed abrupt changes in the SFG spectra of water at electrode surfaces under extremely high field conditions indicating that water possesses an asymmetric dielectric response and, thus, interfacial water cannot be treated as a simple dielectric medium.[10,11] In a similar study, Wang et al. performed SFG spectroscopy on CaF_2-supported graphene under applied potentials and attributed the OH peak formation to electrochemically driven Ca−OH bond formation.[12,13] Li et al. reported that interfacial water undergoes evolution in configuration from parallel to one hydrogen atom facing the electrode to two hydrogen atoms facing the electrodes while an external potential is applied.[14] Poli et al. showed that small amounts of charge transfers along hydrogen bonds, while disparities in the hydrogen bond network resulting from topological defects can cause negative surface charge to accumulate at both interfaces.[15] In the work presented here, we seek to better understand the electrochemical properties of the graphene/water interface in the extremely low applied potential regime. Recent advancements have focused on utilizing pure H_2O as an electrolyte in various electrochemical applications, particularly in piezocatalysis and supercapacitors.[16−18] and the work reported here could be applicable to these fields. Although these results may not lead to more efficient catalytic processes, they are of interest from a fundamental science perspective, as several research groups have recently studied the structure of water at a graphene interface as a function of electrode potential.[19−21] Since its discovery, graphene has been extensively used in electrochemical devices such as sensors,[22−25] capacitors,[26−30] supercapacitors,[31−33] batteries,[34,35] and solar cells.[36−38] A key

Received: June 10, 2024
Revised: August 9, 2024
Accepted: August 13, 2024

challenge of supercapacitors is enabling a wide voltage window, and graphene-based electrodes have shown promising results so far in this area. Single layer graphene on insulating surfaces has been proven to be transparent to hydrogen evolution reaction (HER) electrons.[39] Raman spectroscopy is a useful tool to monitor the stability of graphene, as well as its surface charge density. Zhou et al. studied the potential dependent Raman spectra of graphene on various substrates and found a metal substrate-induced blueshift in the 2D band due to dielectric screening.[40] Zhong et al. found that the interfacial capacitance of graphene has a strong dependence on its charge concentration, which can be probed by the ratio of the 2D band and G band Raman intensities.[41] Wang et al. showed that the applied potential on graphene triggers the dissociation of water molecules confined between the graphene sheet and CaF_2 substrate while exploring applied potentials limited to above −1.23 V vs Pd/H_2.[12] Kalbac et al. studied the electrochemical doping of CVD-grown graphene and found that, like mechanically exfoliated graphene, CVD-grown graphene also exhibits a strong dependence of the 2D/G band ratio on the applied potential.[42]

Graphene electrodes show a linear G band Raman shift proportional to the applied electrochemical potential, which implies that the interface behaves like a linear capacitor over a surprisingly large potential range.[42−45] Studies on graphene−electrolyte interfaces are typically limited to an electrochemical potential range of $V_{applied}$ = ± 1.5 V vs Ag/AgCl. However, Montenegro et al. studied the graphene−water interface under very low applied potentials of $V_{applied}$ = −3.9 V vs Ag/AgCl, and found graphene to be stable in that potential window due to the hydrophobic and catalytically inert nature of graphene.[10,11] In the work presented here, we study the Raman spectra of graphene under extremely low applied potentials ($V_{applied}$ = −7 V vs Ag/AgCl) to develop an understanding of the unique scenario provided by the graphene electrode at these extremely low applied potentials. By measuring the solution resistance, we are able to separate the reducing potential at the working electrode and the voltage drop across the highly resistive aqueous solution. We have also demonstrated that the choice of substrate and solution is critical in achieving the low reducing potentials which has not been reported in the existing literature.

■ MATERIALS AND METHODS

Here, monolayer graphene is synthesized via chemical vapor deposition (CVD) on copper foil (1 cm × 1.5 cm) using H_2 and CH_4 at flow rates of 50 and 7 sccm, respectively, at a pressure of approximately 1.5 Torr and a temperature of 1000 °C for 40 min (see Figure 1a). Following the growth, a layer of PMMA is spin-coated on the graphene/copper foil, and the copper foil is etched away using a $FeCl_3$ solution. The resulting graphene/PMMA film is then rinsed twice with DI water and soaked in 10% HCl for 20 min to remove any remaining etchant. Subsequently, the sample is rinsed two more times with DI water to remove any residual HCl, leaving the graphene/PMMA film floating on the surface of the DI water due to its hydrophobic nature, as shown in Figure 1b. The film is then transferred (i.e., scooped out) onto a CaF_2 window (1″ diameter x 2 mm, from Thorlabs), baked at 150 °C for 15 min for better adhesion, and subsequently treated with acetone solution to remove the PMMA layer.[46−48] In preparation for transfer, two 50 nm-thick gold strips are deposited onto the CaF_2 window, as depicted in Figure 1c, to facilitate good electrical contact with the graphene and enable the attachment of macroscopic electrodes for electrochemical measurements. The gold films were deposited using electron beam evaporation. A 5 nm Ti layer was used as an adhesion layer to the surface, and the deposition rate was 1 Å/s. Raman spectra of the resulting graphene-on-CaF_2 sample exhibit a 2D/G band Raman intensity ratio of nearly 2, indicating high-quality graphene. The CaF_2-supported graphene electrode serves as the top window of the electrochemical flow cell as shown in Figure 1d. The graphene electrode (working electrode) and glassy carbon electrode (counter electrode) are separated by a hollow, cylindrical Teflon spacer (illustrated in Figure 1d), with the graphene electrode inverted and adjacent to the D_2O, H_2O or ionic liquid (Sigma-Aldrich) media. The same procedure was used to prepare the graphene on glass electrodes to ensure proper comparison between CaF_2 and glass substrates. The glass substrates were standard microscope slides obtained from VWR Inc. Potential-dependent Raman spectra of the graphene electrode's G band (at ∼1585 cm^{-1}) are collected using a Renishaw in Via micro-Raman spectrometer, and a 40× glass correction lens (NA = 0.45) was used to correct for the thickness of the CaF_2 substrate. Spectra were taken with 532 nm wavelength excitation.

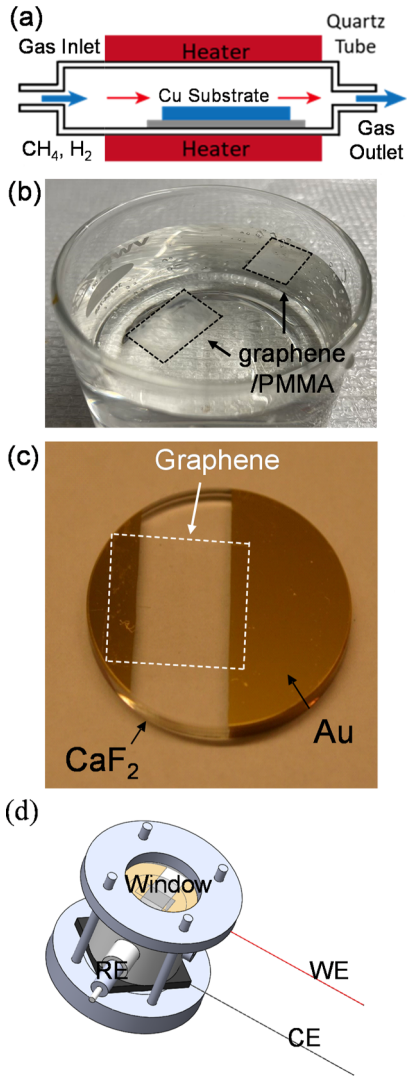

Figure 1. (a) Schematic diagram of the tube furnace used for graphene CVD growth. (b) Photograph of monolayer graphene/PMMA floating on top of DI water prior to transfer onto the CaF_2 substrate. (c) Photograph of the 1″ diameter CaF_2 window with monolayer graphene and Au side electrodes/contacts. (d) Schematic diagram of the electrochemical cell (WE: working electrode, RE: reference electrode, CE: counter electrode).

https://doi.org/10.1021/acsami.4c09551
ACS Appl. Mater. Interfaces XXXX, XXX, XXX−XXX

RESULTS AND DISCUSSION

Figure 2a shows the G band Raman shift of the graphene electrode, which exhibits a linear dependence on the applied

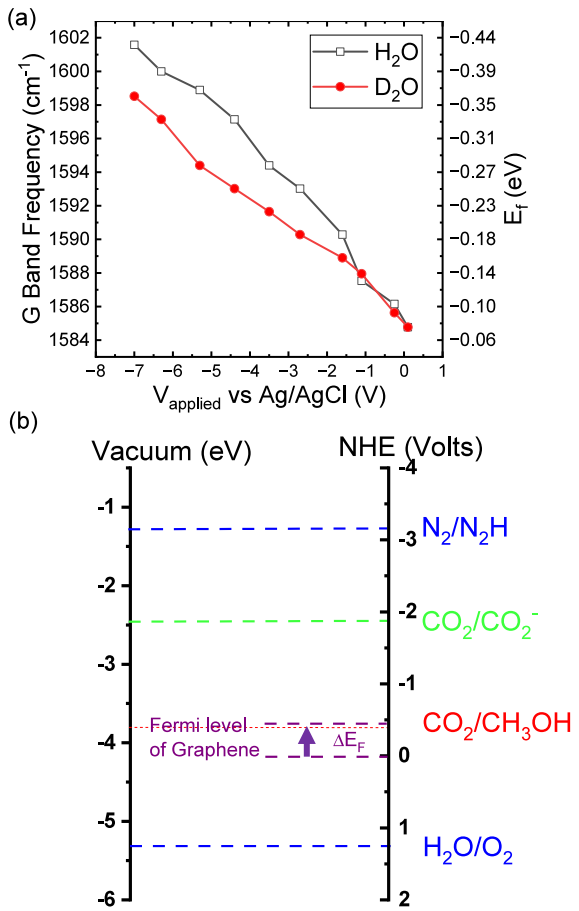

Figure 2. (a) G band Raman frequency and graphene Fermi energy plotted as a function of electrochemical potential (vs Ag/AgCl). (b) Energy band diagram illustrating the change in Fermi energy of the graphene interface where the left axis is expressed with respect to vacuum energy and right axis is expressed with respect to normal hydrogen electrode. The dashed lines represent energy levels of several known half reactions.

electrochemical potential with blueshifts as high as $\Delta\omega_G = 18$ cm^{-1} observed at $V_{applied} = -7$ V vs Ag/AgCl. The G band Raman shift ($\Delta\omega_G$) exhibits a linear response with Fermi level shift, as follows[49,50]

$$\Delta E_F = 21\Delta\omega_G + 75 \quad (1)$$

where $\Delta\omega_G$ is given in units of cm^{-1} and ΔE_F is given in units of meV. The change in Fermi energy of the graphene ΔE_F is plotted on the right y-axis of Figure 2a and spans a range from −0.08 eV (for no applied potential) to −0.43 eV (for the lowest applied potential). This relatively large change in the Fermi energy of the electrode is a direct result of graphene's small density of electronic states, and is not possible in bulk metal electrodes, where any change in the Fermi energy would be negligible. To put this in the context of electrochemistry, Figure 2b shows an energy band diagram illustrating the change in Fermi energy with respect to several common redox potentials. Here, the shift of $\Delta E_F = -0.43$ eV corresponds to a shift in the electrode potential out of equilibrium by −0.43 V, favoring reduction half reactions. It should be noted that the Fermi level shift (ΔE_F) does not change graphene's electronic band structure, instead the primary effect is to change the effective work function of the material, as illustrated in Figure S6.[51]

The linear relationship between the G band shift and the applied potential implies that the interface acts like a linear capacitor. Applying an electrochemical potential to the graphene electrode acts as an electrolyte gate and provides a method to dope the material electrochemically. When an electrochemical potential is applied, charge accumulation on the graphene electrodes shifts the Fermi level of the graphene. Since the G band is linearly proportional to the applied potential, the Fermi level is also linearly proportional to the applied potential.[45] Subsequently, it can also be concluded that the charge density on the graphene surface is linearly proportional to the applied potential. Hence, the graphene water interface acts like a linear capacitor. The amount of charge accumulation on the surface depends on various factors such as the conductivity of the electrolyte, defects in the graphene, the substrate graphene sits on, etc. If a highly resistive electrolyte such as D_2O is used, a higher potential would be required to substantially change the G band frequency. Also, a graphene sheet with a lot of defects will exhibit large D bands when a large reducing potential is applied.

Since both H_2O and D_2O are high impedance solutions, we expect a large voltage drop across the solution. The reducing potential at the electrode is, therefore, not the same as the applied potential. Bonagiri et al. reported charge profiling using three-dimensional (3D) atomic force microscopy (CP-3D-AFM) to experimentally quantify the real-space charge distribution of the electrode surface and electric double layers (EDLs) with angstrom depth resolution, and found that these charged interfacial layers extend over approximately 1 nm.[52,53] Furthermore, Fumagalli et al. showed that confined water at the electrode-liquid interface has an anomalously low dielectric constant.[54] Bonthuis et al. also demonstrated that the capacitance at the interface is lower than the bulk due to the lower dielectric constant of interfacial water.[55] Thus, it is crucial to isolate the effect of EDL and bulk solution resistance. The voltage step method (VSM) was employed to determine the solution resistance where first 0 V is applied, and after 10 ms, a potential step of −1 V was applied, as illustrated in Figures 3a and S1. Since it is an abrupt potential change, and the electrochemical double layer capacitor is uncharged (i.e., functions as a short circuit at the instant the voltage step is applied), the solution resistance is the only impedance in the whole circuit. The solution resistance R is equal to $V/\Delta I$, where ΔI is the change in current at the instant the potential step is applied (see Figure 3a). From these voltage step measurements, the solution resistances of D_2O, H_2O, and ionic liquid were determined to be 18 kΩ, 12.3 kΩ, and 718 Ω, respectively. Figure 3b shows a plot of the voltage drop across the solution (i.e., V_{IR}) based on these resistance values. Figure 3c shows a plot of the effective reducing potential (i.e., V_{eff}) plotted as a function of the applied potential $V_{applied}$, showing a minimum value of $V_{eff} = -3.9$ V vs Ag/AgCl for D_2O. The corresponding G band Raman shifts and current densities are plotted in Figure S7a,b. The current densities are very low (<300 μA/cm^2 in H_2O and <200 μA/cm^2 in D_2O). One of the reasons for the low current density is the 0.3 nm gap between the graphene surface and the electrolyte.[10,11] The small vacuum gap decreases the interfacial capacitance and decreases

https://doi.org/10.1021/acsami.4c09551
ACS Appl. Mater. Interfaces XXXX, XXX, XXX−XXX

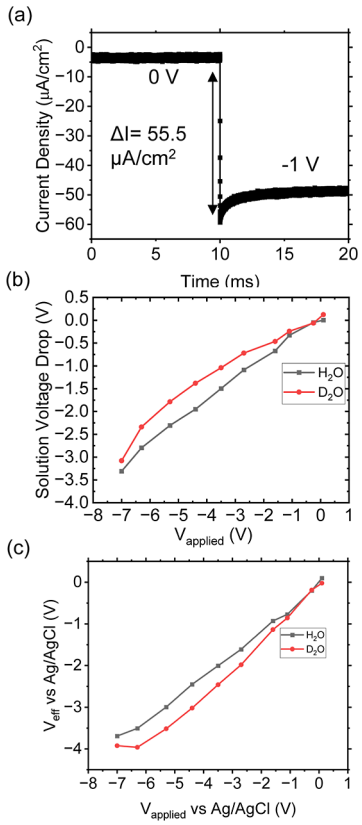

Figure 3. (a) Solution resistance measurement of D_2O using the voltage step method. (b) Solution voltage drop as a function of applied potential. (c) The effective electrochemical potential at the electrode, V_{eff} as a function of applied potential.

the current density when a potential is applied. The low current density in D_2O originates from the higher purity and slower ion kinetics than H_2O.[56] Another possible reason could be differences in local pH and pD. The local pH at graphene/DI water interfaces has been previously reported using surface-enhanced Raman spectroscopy measurements,[46] and it could be interesting to measure the local pD under these extremely low reducing potentials. Furthermore, previous reports indicate that reactions are slower with D_2O than with H_2O due to kinetic isotope effects. Hence, the kinetic isotope effect could help improve the electrochemical stability of CaF_2-supported graphene electrodes in contact with D_2O compared with H_2O.[57,58] D_2O and H_2O both have lower current densities than ionic liquid because of the instability of ionic liquids below −2.7 V vs Ag/AgCl. The low current densities indicate that the rate of the hydrogen evolution reaction (HER) is very low at the electrode surface. Due to the low rate of HER, we observe minimal bubble formation. Thus, we could perform Raman spectroscopy at low reducing potentials, and the spectra's intensity and signal-to-noise ratio (SNR) were unaffected down to −7 V vs Ag/AgCl. Another method of determining the solution resistance is electronic impedance spectroscopy (EIS). A complete set of EIS measurements for the CaF_2-supported graphene electrode are shown in Figure S5 of the Supporting Information document. In the low-frequency regime, the EDL capacitance is negligible, however, the EIS measurements produce a negative impedance in this regime. The negative impedance arises from parasitic inductance in the external circuit—an effect that is more pronounced because of the high impedance of the solution. In the high-frequency regime, the EIS measurement yields a voltage-dependent solution resistance in the range of 30−50 kΩ, as shown in Figure S5. These values are somewhat higher than the 20 kΩ value obtained via the VSM measurement. We believe that the VSM value (i.e., 20 kΩ) is more reliable than that of the EIS measurements because the left intercept of the EIS curve is negative, due to the parasitic inductance of the potentiostat. Usually, the inductance does not affect EIS measurements in low-resistance solutions. However, in this case, the inductance causes the left intercept to become negative. The left intercept is constant, while the right intercept is potential dependent, which shows that the solution resistance is constant, and the EDL capacitance is solution dependent. In the voltage step method, there is no EDL capacitance due to the sharp rise in voltage, and we can measure the solution resistance accurately. Therefore, we prefer the voltage step method over the EIS approach.

As a comparison to the D_2O and H_2O solutions, we measured Raman spectra of the CaF2-supported graphene electrode in ionic liquid [DEME][TFSI] under various applied potentials. As shown in Figure 4a, the G band Raman

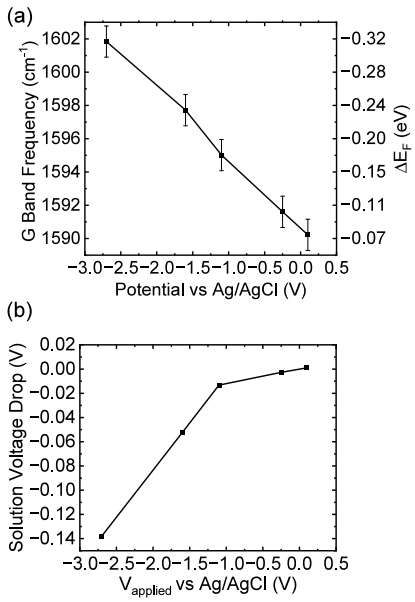

Figure 4. (a) Potential dependent G band frequency and Fermi level of graphene in [DEME][TFSI] ionic liquid. (b) Voltage drop (V_{IR}) across the solution plotted as a function of applied potential.

frequency exhibits a linear relationship with the applied potential. However, the current density increases significantly below $V_{applied}$ = −1.1 V vs Ag/AgCl, as shown in Figure S8a. The current density becomes greater than 200 $\mu A/cm^2$ at $V_{applied}$ = −2.7 V vs Ag/AgCl. On the contrary, when D_2O is used as an electrolyte, the value of current density stays below this limit (i.e., 200 $\mu A/cm^2$) even at $V_{applied}$ = −7 V vs Ag/AgCl. The voltage step measurements on ionic liquids show that ionic liquids have much smaller resistance than D_2O or H_2O, as expected, with voltage drops across the solution of only 0.14 V at −2.7 V applied potential vs Ag/AgCl, as shown in Figure 4b. Although the TFSI ionic liquids have one of the widest electrochemical stability ranges, we find that it starts to break down beyond −2.7 V vs Ag/AgCl, which is in good agreement with previously reported literature.[59] Nevertheless,

https://doi.org/10.1021/acsami.4c09551
ACS Appl. Mater. Interfaces XXXX, XXX, XXX−XXX

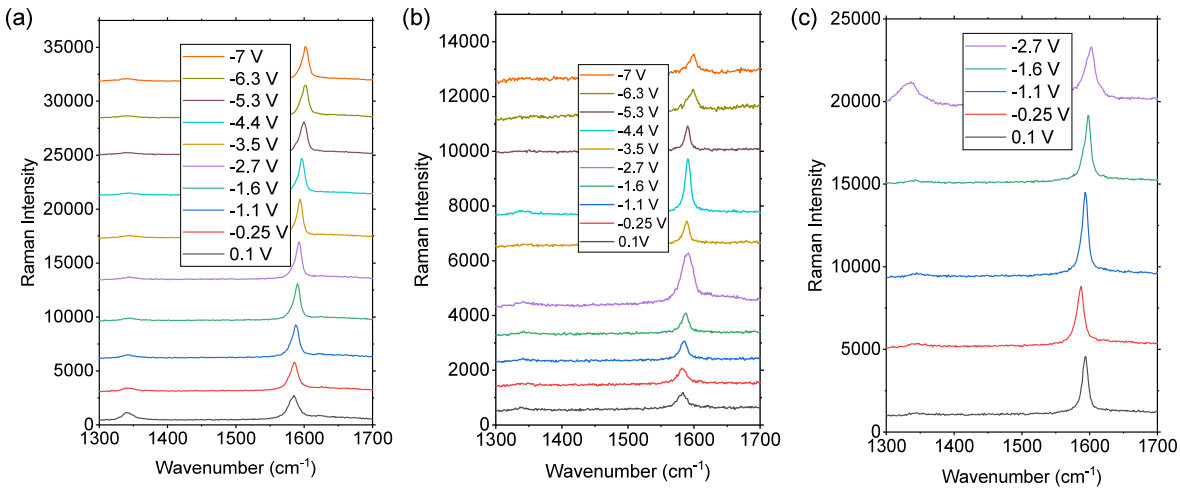

Figure 5. Comparison of the Raman spectra of (a) CaF_2, (b) BK-7, and (c) glass slide supported graphene taken under different applied electrochemical potentials using H_2O as the solution.

the effective reducing potential with ionic liquid [DEME]-[TFSI] as an electrolyte is $V_{eff} = -2.56$ V vs Ag/AgCl, which is not as low as the reducing potential achieved with D_2O. In addition, the change in Fermi level (ΔE_F) reaches 0.32 eV at this low reducing potential, as plotted in Figure 4a.

The Raman spectra are also used to detect degradation of the electrode under these large reducing potentials. We find that these electrodes can support $V_{applied} = -7$ V vs Ag/AgCl without causing a D band to form, as plotted in Figures 5a and S3. Additional data sets of Raman spectra of graphene on CaF_2 substrates are presented on Figure S9. However, oxidative potentials above $V_{applied} = +0.5$ V vs Ag/AgCl do result in the formation of a substantial D band, indicating that these graphene-based electrodes are more robust to reducing potentials than oxidative potentials. The CaF_2 supporting substrate is important for achieving low reducing potentials without causing a D band, since CaF_2 has significantly lower trapped charges and impurities than other substrates such as glass. Recent reports have indicated that CaF_2 is an outstanding choice as a substrate material for 2D material electronics due to its high dielectric constant, inert nature, and lack of charge traps.[60−62] CaF_2 supported graphene has also been used extensively to study graphene−water interfaces.[10,11,13] The fluorine termination layer in CaF_2 results in the absence of dangling bonds, which results in enhanced stability, and lack of trapped charges at the surface. The high-quality Raman spectra of CaF_2 supported graphene is in good agreement with the literature. Graphene-on-glass electrodes show severe degradation and the emergence of a strong D band Raman mode at potentials below $V_{applied} = -2.7$ V vs Ag/AgCl, as shown in Figures 5c and S4. This indicates that the defects, impurities, and trapped charge in the glass facilitate the electrochemically driven corrosion of the graphene interface. Defects in the graphene surface provide catalytically active sites and enhance the reaction with water molecules.[63] Consequently,CaF_2 provides a better substrate compared to glass in terms of stability when subjected to applied potentials. CaF_2 also performed better than the BK-7 substrates (from Thorlabs Inc.). While there is no prominent D band formation when extremely low reducing potentials are applied to CaF_2 or BK-7, the currents are significantly higher for BK-7 supported graphene. The current reaches −7.43 mA on BK-7, whereas the current does not exceed 270 μA with CaF_2 as the substrate. Hence CaF_2 is the ideal substrate for achieving low reducing potentials.

CONCLUSIONS

Our study presents electrochemical measurements using in situ Raman spectroscopy at interfaces between CaF_2-supported graphene and water (H_2O and D_2O) under extremely low applied potentials. By leveraging graphene's hydrophobic and noncatalytic properties, water's insulating nature, and the inert properties of CaF_2 substrates, we successfully apply potentials as low as $V_{applied} = -7$ V vs Ag/AgCl while maintaining current densities below 200 μA/cm^2, which enables in situ spectra to be obtained reliably over this wide potential range. We compared CaF_2 substrates with standard microscope glass slide substrates. CaF_2 substrates enable lower reducing potentials without causing D band formation in graphene due to the lack of trapped charges in CaF_2. For further comparison, we also tested BK-7 as a substrate. BK-7 proved to be a better substrate than glass slides but performed worse than CaF_2, in terms of stability. Furthermore, D_2O proved to enable lower reducing potentials due to its purity and high impedance. Solution resistance measurements demonstrated that, although the solution voltage drop is higher for high-impedance solutions, the reducing potential is still more negative than what can be achieved with low-impedance solutions, such as ionic liquids. We determined the solution resistances of D_2O, H_2O, and ionic liquid to be 18 kΩ, 12.3 kΩ, and 718 Ω, respectively, corresponding to minimum effective reducing potentials of 3.9, 3.69, and 2.56 V, respectively.

ASSOCIATED CONTENT

Supporting Information

The Supporting Information is available free of charge at https://pubs.acs.org/doi/10.1021/acsami.4c09551.

Additional details for solution resistance measurement; plot of 2D/G band ratio as a function of applied potential and G band frequency; additional data set of Raman spectra of graphene on various substrates; current density as a function of applied potential for various substrates and solutions; AFM and SEM images of the graphene electrodes (PDF)

https://doi.org/10.1021/acsami.4c09551
ACS Appl. Mater. Interfaces XXXX, XXX, XXX−XXX

AUTHOR INFORMATION

Corresponding Author

Stephen B. Cronin − *Ming Hsieh Department of Electrical Engineering, University of Southern California, Los Angeles, California 90089, United States; Department of Physics and Astronomy and Department of Chemistry, University of Southern California, Los Angeles, California 90089, United States;* orcid.org/0000-0001-9153-7687; Email: scronin@usc.edu

Authors

Rifat Shahriar − *Ming Hsieh Department of Electrical Engineering, University of Southern California, Los Angeles, California 90089, United States;* orcid.org/0000-0003-1245-6753

Bofan Zhao − *Ming Hsieh Department of Electrical Engineering, University of Southern California, Los Angeles, California 90089, United States;* orcid.org/0000-0003-0478-6330

Indu Aravind − *Department of Physics and Astronomy, University of Southern California, Los Angeles, California 90089, United States;* orcid.org/0000-0002-0908-9887

Zhi Cai − *Mork Family Department of Chemical Engineering and Materials Science, University of Southern California, Los Angeles, California 90089, United States;* orcid.org/0000-0002-3741-5715

Yu Yun Wang − *Ming Hsieh Department of Electrical Engineering, University of Southern California, Los Angeles, California 90089, United States;* orcid.org/0000-0003-0620-5069

Boxin Zhang − *Mork Family Department of Chemical Engineering and Materials Science, University of Southern California, Los Angeles, California 90089, United States*

Complete contact information is available at: https://pubs.acs.org/10.1021/acsami.4c09551

Notes

The authors declare no competing financial interest.

ACKNOWLEDGMENTS

This research was supported by the U.S. Department of Energy, Office of Basic Energy Sciences award no. DESC0019322 (R.S.); the Army Research Office (ARO) award no. W911NF-22-1−0284 (I.A.); Office of Naval Research (ONR) Award no. N000142212697 (Z.C.), National Science Foundation (NSF) award no. CBET-2012845 (B.Z.) and Air Force Office of Scientific Research (AFOSR) grant no. FA9550-19-1-0115 (B.Z.).

REFERENCES

(1) Zhang, M.; Hao, H.; Zhou, D.; Duan, Y.; Wang, Y.; Bian, H. Understanding the Microscopic Structure of a "Water-in-Salt" Lithium Ion Battery Electrolyte Probed with Ultrafast IR Spectroscopy. *J. Phys. Chem. C* **2020**, *124*, 8594−8604.

(2) Fayer, M. D. Dynamics of Water Interacting with Interfaces, Molecules, and Ions. *Acc. Chem. Res.* **2012**, *45*, 3−14.

(3) Toney, M. F.; Howard, J. N.; Richer, J.; Borges, G. L.; Gordon, J. G.; Melroy, O. R.; Wiesler, D. G.; Yee, D.; Sorensen, L. B. Voltage-dependent ordering of water molecules at an electrode−electrolyte interface. *Nature* **1994**, *368*, 444−446.

(4) Singh, P. C.; Nihonyanagi, S.; Yamaguchi, S.; Tahara, T. Interfacial water in the vicinity of a positively charged interface studied by steady-state and time-resolved heterodyne-detected vibrational sum frequency generation. *J. Chem. Phys.* **2014**, *141*, 18C527.

(5) Dutta, C.; Svirida, A.; Mammetkuliyev, M.; Rukhadze, M.; Benderskii, A. V. Insight into Water Structure at the Surfactant Surfaces and in Microemulsion Confinement. *J. Phys. Chem. B* **2017**, *121*, 7447−7454.

(6) Dutta, C.; Mammetkuliyev, M.; Benderskii, A. V. Re-orientation of water molecules in response to surface charge at surfactant interfaces. *J. Chem. Phys.* **2019**, *151*, 034703.

(7) Singh, P. C.; Nihonyanagi, S.; Yamaguchi, S.; Tahara, T. Ultrafast vibrational dynamics of water at a charged interface revealed by two-dimensional heterodyne-detected vibrational sum frequency generation. *J. Chem. Phys.* **2012**, *137*, 094706.

(8) Nihonyanagi, S.; Yamaguchi, S.; Tahara, T. Direct evidence for orientational flip-flop of water molecules at charged interfaces: A heterodyne-detected vibrational sum frequency generation study. *J. Chem. Phys.* **2009**, *130*, 204704.

(9) Rehl, B.; Ma, E.; Parshotam, S.; DeWalt-Kerian, E. L.; Liu, T.; Geiger, F. M.; Gibbs, J. M. Water Structure in the Electrical Double Layer and the Contributions to the Total Interfacial Potential at Different Surface Charge Densities. *J. Am. Chem. Soc.* **2022**, *144*, 16338−16349.

(10) Montenegro, A.; Dutta, C.; Mammetkuliev, M.; Shi, H. T.; Hou, B. Y.; Bhattacharyya, D.; Zhao, B. F.; Cronin, S. B.; Benderskii, A. V. Asymmetric response of interfacial water to applied electric fields. *Nature* **2021**, *594*, 62−65.

(11) Montenegro, A.; Vaughn, A. E.; Mammetkuliyev, M.; Zhao, B.; Zhang, B.; Shi, H.; Bhattacharyya, D.; Benderskii, A. V.; Cronin, S. B. Field-Dependent Orientation and Free Energy of D_2O at an Electrode Surface Observed via SFG Spectroscopy. *J. Phys. Chem. C* **2022**, *126*, 20831−20839.

(12) Wang, Y.; Seki, T.; Liu, X.; Yu, X.; Yu, C.-C.; Domke, K. F.; Hunger, J.; Koper, M. T. M.; Chen, Y.; Nagata, Y.; Bonn, M. Direct Probe of Electrochemical Pseudocapacitive pH Jump at a Graphene Electrode. *Angew. Chem., Int. Ed.* **2023**, *62*, No. e202216604.

(13) Wang, Y.; Seki, T.; Yu, X.; Yu, C.-C.; Chiang, K.-Y.; Domke, K. F.; Hunger, J.; Chen, Y.; Nagata, Y.; Bonn, M. Chemistry governs water organization at a graphene electrode. *Nature* **2023**, *615*, E1−E2.

(14) Li, C.-Y.; Le, J.-B.; Wang, Y.-H.; Chen, S.; Yang, Z.-L.; Li, J.-F.; Cheng, J.; Tian, Z.-Q. In situ probing electrified interfacial water structures at atomically flat surfaces. *Nat. Mater.* **2019**, *18*, 697−701.

(15) Poli, E.; Jong, K. H.; Hassanali, A. Charge transfer as a ubiquitous mechanism in determining the negative charge at hydrophobic interfaces. *Nat. Commun.* **2020**, *11*, 901.

(16) Feng, W.; Yuan, J.; Zhang, L.; Hu, W.; Wu, Z.; Wang, X.; Huang, X.; Liu, P.; Zhang, S. Atomically thin ZnS nanosheets: Facile synthesis and superior piezocatalytic H_2 production from pure H_2O. *Appl. Catal. B Environ.* **2020**, *277*, 119250.

(17) Huettner, C.; Xu, F.; Paasch, S.; Kensy, C.; Zhai, Y. X.; Yang, J.; Brunner, E.; Kaskel, S. Ultra-hydrophilic porous carbons and their supercapacitor performance using pure water as electrolyte. *Carbon* **2021**, *178*, 540−551.

(18) Zhao, Y.; Fang, Z.-B.; Feng, W.; Wang, K.; Huang, X.; Liu, P. Hydrogen Production from Pure Water via Piezoelectric-assisted Visible-light Photocatalysis of CdS Nanorod Arrays. *ChemCatChem* **2018**, *10*, 3397−3401.

(19) Li, X.; Li, L.; Wang, Y.; Li, H.; Bian, X. Wetting and Interfacial Properties of Water on the Defective Graphene. *J. Phys. Chem. C* **2013**, *117*, 14106−14112.

(20) Zhang, Y.; de Aguiar, H. B.; Hynes, J. T.; Laage, D. Water Structure, Dynamics, and Sum-Frequency Generation Spectra at Electrified Graphene Interfaces. *J. Phys. Chem. Lett.* **2020**, *11*, 624−631.

(21) Ma, Y.; Zhang, Z.; Chen, J.; Sääskilahti, K.; Volz, S.; Chen, J. Ordered water layers by interfacial charge decoration leading to an ultra-low Kapitza resistance between graphene and water. *Carbon* **2018**, *135*, 263−269.

(22) Yoon, H. J.; Jun, D. H.; Yang, J. H.; Zhou, Z.; Yang, S. S.; Cheng, M. M.-C. Carbon dioxide gas sensor using a graphene sheet. *Sens. Actuators, B* **2011**, *157*, 310−313.
(23) Chung, M. G.; Kim, D. H.; Lee, H. M.; Kim, T.; Choi, J. H.; Seo, D. k.; Yoo, J. B.; Hong, S. H.; Kang, T. J.; Kim, Y. H. Highly sensitive NO_2 gas sensor based on ozone treated graphene. *Sens. Actuators, B* **2012**, *166−167*, 172−176.
(24) Jiang, G.; Goledzinowski, M.; Comeau, F. J.; Zarrin, H.; Lui, G.; Lenos, J.; Veileux, A.; Liu, G.; Zhang, J.; Hemmati, S.; et al. Free-standing functionalized graphene oxide solid electrolytes in electrochemical gas sensors. *Adv. Funct. Mater.* **2016**, *26*, 1729−1736.
(25) Tang, X.; Mager, N.; Vanhorenbeke, B.; Hermans, S.; Raskin, J.-P. Defect-free functionalized graphene sensor for formaldehyde detection. *Nanotechnology* **2017**, *28*, 055501.
(26) Deng, L.; Zhu, G.; Wang, J.; Kang, L.; Liu, Z.-H.; Yang, Z.; Wang, Z. Graphene−MnO_2 and graphene asymmetrical electrochemical capacitor with a high energy density in aqueous electrolyte. *J. Power Sources* **2011**, *196*, 10782−10787.
(27) Feng, G.; Li, S.; Presser, V.; Cummings, P. T. Molecular Insights into Carbon Supercapacitors Based on Room-Temperature Ionic Liquids. *J. Phys. Chem. Lett.* **2013**, *4*, 3367−3376.
(28) Kim, W.; Joo, J. B.; Kim, N.; Oh, S.; Kim, P.; Yi, J. Preparation of nitrogen-doped mesoporous carbon nanopipes for the electrochemical double layer capacitor. *Carbon* **2009**, *47*, 1407−1411.
(29) Miller, J. R.; Outlaw, R.; Holloway, B. Graphene double-layer capacitor with ac line-filtering performance. *Science* **2010**, *329*, 1637−1639.
(30) Miller, J. R.; Outlaw, R.; Holloway, B. Graphene electric double layer capacitor with ultra-high-power performance. *Electrochim. Acta* **2011**, *56*, 10443−10449.
(31) Cao, J.; Wang, Y.; Zhou, Y.; Ouyang, J.-H.; Jia, D.; Guo, L. High voltage asymmetric supercapacitor based on MnO_2 and graphene electrodes. *J. Electroanal. Chem.* **2013**, *689*, 201−206.
(32) Yang, H.; Kannappan, S.; Pandian, A. S.; Jang, J.-H.; Lee, Y. S.; Lu, W. Graphene supercapacitor with both high power and energy density. *Nanotechnology* **2017**, *28*, 445401.
(33) Zhao, B.; Liu, P.; Jiang, Y.; Pan, D.; Tao, H.; Song, J.; Fang, T.; Xu, W. Supercapacitor performances of thermally reduced graphene oxide. *J. Power Sources* **2012**, *198*, 423−427.
(34) Kim, H.; Park, K.-Y.; Hong, J.; Kang, K. All-graphene-battery: bridging the gap between supercapacitors and lithium ion batteries. *Sci. Rep.* **2014**, *4*, 5278.
(35) Xu, H.; Chen, H.; Lai, H.; Li, Z.; Dong, X.; Cai, S.; Chu, X.; Gao, C. Capacitive charge storage enables an ultrahigh cathode capacity in aluminum-graphene battery. *J. Energy Chem.* **2020**, *45*, 40−44.
(36) Casaluci, S.; Gemmi, M.; Pellegrini, V.; Di Carlo, A.; Bonaccorso, F. Graphene-based large area dye-sensitized solar cell modules. *Nanoscale* **2016**, *8*, 5368−5378.
(37) Li, X.; Zhu, H.; Wang, K.; Cao, A.; Wei, J.; Li, C.; Jia, Y.; Li, Z.; Li, X.; Wu, D. Graphene-on-silicon Schottky junction solar cells. *Adv. Mater.* **2010**, *22*, 2743−2748.
(38) Miao, X.; Tongay, S.; Petterson, M. K.; Berke, K.; Rinzler, A. G.; Appleton, B. R.; Hebard, A. F. High efficiency graphene solar cells by chemical doping. *Nano Lett.* **2012**, *12*, 2745−2750.
(39) Xie, A.; Xuan, N.; Ba, K.; Sun, Z. Pristine Graphene Electrode in Hydrogen Evolution Reaction. *ACS Appl. Mater. Interfaces* **2017**, *9*, 4643−4648.
(40) Zhou, R.; Yasuda, S.; Minamimoto, H.; Murakoshi, K. Sensitive Raman Probe of Electronic Interactions between Monolayer Graphene and Substrate under Electrochemical Potential Control. *ACS Omega* **2018**, *3*, 2322−2328.
(41) Zhong, J.-H.; Liu, J.-Y.; Li, Q.; Li, M.-G.; Zeng, Z.-C.; Hu, S.; Wu, D.-Y.; Cai, W.; Ren, B. Interfacial capacitance of graphene: Correlated differential capacitance and in situ electrochemical Raman spectroscopy study. *Electrochim. Acta* **2013**, *110*, 754−761.
(42) Kalbac, M.; Reina-Cecco, A.; Farhat, H.; Kong, J.; Kavan, L.; Dresselhaus, M. S. The Influence of Strong Electron and Hole Doping on the Raman Intensity of Chemical Vapor-Deposition Graphene. *ACS Nano* **2010**, *4*, 6055−6063.
(43) Ferrari, A. C.; Basko, D. M. Raman spectroscopy as a versatile tool for studying the properties of graphene. *Nat. Nanotechnol.* **2013**, *8*, 235−246.
(44) Frank, O.; Dresselhaus, M. S.; Kalbac, M. Raman Spectroscopy and in Situ Raman Spectroelectrochemistry of Isotopically Engineered Graphene Systems. *Acc. Chem. Res.* **2015**, *48*, 111−118.
(45) Das, A.; Pisana, S.; Chakraborty, B.; Piscanec, S.; Saha, S. K.; Waghmare, U. V.; Novoselov, K. S.; Krishnamurthy, H. R.; Geim, A. K.; Ferrari, A. C.; Sood, A. K. Monitoring dopants by Raman scattering in an electrochemically top-gated graphene transistor. *Nat. Nanotechnol.* **2008**, *3*, 210−215.
(46) Shi, H.; Poudel, N.; Hou, B.; Shen, L.; Chen, J.; Benderskii, A. V.; Cronin, S. B. Sensing local pH and ion concentration at graphene electrode surfaces using in situ Raman spectroscopy. *Nanoscale* **2018**, *10*, 2398−2403.
(47) Shi, H.; Zhao, B.; Ma, J.; Bronson, M. J., Jr.; Cai, Z.; Chen, J.; Wang, Y.; Cronin, M.; Jensen, L.; Cronin, S. B. Measuring Local Electric Fields and Local Charge Densities at Electrode Surfaces Using Graphene-Enhanced Raman Spectroscopy (GERS)-Based Stark-Shifts. *ACS Appl. Mater. Interfaces* **2019**, *11*, 36252−36258.
(48) Chae, H. U.; Ahsan, R.; Tao, J.; Cronin, S. B.; Kapadia, R. Tunable Onset of Hydrogen Evolution in Graphene with Hot Electrons. *Nano Lett.* **2020**, *20*, 1791−1799.
(49) Das Sarma, S.; Adam, S.; Hwang, E. H.; Rossi, E. Electronic transport in two-dimensional graphene. *Rev. Mod. Phys.* **2011**, *83*, 407−470.
(50) Froehlicher, G.; Berciaud, S. Raman spectroscopy of electrochemically gated graphene transistors: Geometrical capacitance, electron-phonon, electron-electron, and electron-defect scattering. *Phys. Rev. B* **2015**, *91*, 205413.
(51) Cai, Z.; Aravind, I.; Weinstein, H.; Li, R.; Wu, J.; Wang, H.; Habif, J.; Cronin, S. Gate-tunable modulation of the optical properties of multilayer graphene by the reversible intercalation of ionic liquid anions. *J. Appl. Phys.* **2022**, *132*, 095102.
(52) Bonagiri, L. K. S.; Panse, K. S.; Zhou, S.; Wu, H.; Aluru, N. R.; Zhang, Y. Real-Space Charge Density Profiling of Electrode−Electrolyte Interfaces with Angstrom Depth Resolution. *ACS Nano* **2022**, *16*, 19594−19604.
(53) Panse, K. S.; Wu, H.; Zhou, S.; Zhao, F.; Aluru, N. R.; Zhang, Y. Innermost Ion Association Configuration Is a Key Structural Descriptor of Ionic Liquids at Electrified Interfaces. *J. Phys. Chem. Lett.* **2022**, *13*, 9464−9472.
(54) Fumagalli, L.; Esfandiar, A.; Fabregas, R.; Hu, S.; Ares, P.; Janardanan, A.; Yang, Q.; Radha, B.; Taniguchi, T.; Watanabe, K.; Gomila, G.; Novoselov, K. S.; Geim, A. K. Anomalously low dielectric constant of confined water. *Science* **2018**, *360*, 1339−1342.
(55) Bonthuis, D. J.; Gekle, S.; Netz, R. R. Dielectric Profile of Interfacial Water and its Effect on Double-Layer Capacitance. *Phys. Rev. Lett.* **2011**, *107*, 166102.
(56) Thomas, J. J.; Jennings, H. M. Effects of D_2O and mixing on the early hydration kinetics of tricalcium silicate. *Chem. Mater.* **1999**, *11*, 1907−1914.
(57) Fletcher, A. J.; Thomas, K. M. Kinetic Isotope Quantum Effects in the Adsorption of H_2O and D_2O on Porous Carbons. *J. Phys. Chem. C* **2007**, *111*, 2107−2115.
(58) Yates, J. T., Jr.; McKee, D. W. Kinetic isotope effect in the heterogeneous reaction of graphite with H_2O (D_2O). *J. Chem. Phys.* **1981**, *75*, 2711−2714.
(59) Sato, T.; Masuda, G.; Takagi, K. Electrochemical properties of novel ionic liquids for electric double layer capacitor applications. *Electrochim. Acta* **2004**, *49*, 3603−3611.
(60) Chau, T. K.; Suh, D. Graphene Field-Effect Transistor on a Calcium Fluoride Substrate. *J. Korean Phys. Soc.* **2020**, *77*, 879−883.
(61) Koma, A.; Saiki, K.; Sato, Y. Heteroepitaxy of a two-dimensional material on a three-dimensional material. *Appl. Surf. Sci.* **1990**, *41−42*, 451−456.

https://doi.org/10.1021/acsami.4c09551
ACS Appl. Mater. Interfaces XXXX, XXX, XXX−XXX

(62) Wen, C.; Lanza, M. Calcium fluoride as high-k dielectric for 2D electronics. *Applied Physics Reviews* **2021**, *8*, 021307.
(63) Wang, X.; Zhang, J.; Wang, H.; Liang, M.; Wang, Q.; Chen, F. Revealing the Role of Defect in 3D Graphene-Based Photocatalytic Composite for Efficient Elimination of Antibiotic and Heavy Metal Combined Pollution. *Energy Environ. Mater.* **2024**, *7*, No. e12616.

https://doi.org/10.1021/acsami.4c09551
ACS Appl. Mater. Interfaces XXXX, XXX, XXX−XXX